Electrophysiological signature of homomeric and heteromeric glycine receptor channels

Raltschev, C. and Hetsch, F. and Winkelmann, A. and Meier, J.C. and Semtner, M.

Journal of Biological Chemistry
2016 AUG 19 ; 291(34): 18030-18040
Doi: 10.1074/jbc.M116.735084

Publisher: American Society for Biochemistry and Molecular Biology

THE JOURNAL OF BIOLOGICAL CHEMISTRY VOL. 291, NO. 34, pp. 18030–18040, August 19, 2016

Electrophysiological Signature of Homomeric and Heteromeric Glycine Receptor Channels*

Received for publication, April 26, 2016, and in revised form, July 1, 2016 Published, JBC Papers in Press, July 5, 2016, DOI 10.1074/jbc.M116.735084

Constanze Raltschev[‡1], Florian Hetsch[§], Aline Winkelmann[§], Jochen C. Meier[§2,3], and Marcus Semtner[¶2,4]

From the [‡]Department of Biomedicine, Cellular Neurophysiology, University of Basel, Pestalozzistrasse 20, 4056 Basel, Switzerland, the [§]Division of Cell Physiology, Technische Universität Braunschweig, Spielmannstrasse 7, 38106 Braunschweig, Germany, and [¶]Cellular Neurosciences, Max-Delbrück-Centrum für Molekulare Medizin (MDC), Robert-Rössle-Strasse 10, 13092 Berlin, Germany

Glycine receptors are chloride-permeable, ligand-gated ion channels and contribute to the inhibition of neuronal firing in the central nervous system or to facilitation of neurotransmitter release if expressed at presynaptic sites. Recent structure-function studies have provided detailed insights into the mechanisms of channel gating, desensitization, and ion permeation. However, most of the work has focused only on comparing a few isoforms, and among studies, different cellular expression systems were used. Here, we performed a series of experiments using recombinantly expressed homomeric and heteromeric glycine receptor channels, including their splice variants, in the same cellular expression system to investigate and compare their electrophysiological properties. Our data show that the current-voltage relationships of homomeric channels formed by the α2 or α3 subunits change upon receptor desensitization from a linear to an inwardly rectifying shape, in contrast to their heteromeric counterparts. The results demonstrate that inward rectification depends on a single amino acid (Ala^{254}) at the inner pore mouth of the channels and is closely linked to chloride permeation. We also show that the current-voltage relationships of glycine-evoked currents in primary hippocampal neurons are inwardly rectifying upon desensitization. Thus, the alanine residue Ala^{254} determines voltage-dependent rectification upon receptor desensitization and reveals a physio-molecular signature of homomeric glycine receptor channels, which provides unprecedented opportunities for the identification of these channels at the single cell level.

Glycine receptors (GlyRs)[5] are chloride-permeable, ligand-gated ion channels (LGICs) that contribute to synaptic communication in the central nervous system (1, 2). GlyRs are involved in locomotion and the processing of visual, acoustic, and sensory signals. Aberrant function is associated with neuropathic pain and hyperekplexia (startle disease) as well as the pathophysiology of temporal lobe epilepsy and autism spectrum disorder (3–7). The family of GlyRs comprises five genes in humans: *GLRA1–4*, coding for the subunits GlyR α1–4, and *GLRB*, coding for GlyR β (2, 8). Each GlyR subunit is composed of four transmembrane domains (TM1–4) and extracellular N and C termini. Amino acids contributing to the glycine binding site are located in the large extracellular N-terminal domain, whereas the intracellular linker between TM3 and TM4 hosts several signaling domains and phosphorylation sites (8). Functional GlyR channels are either homopentamers formed by five identical α subunits or heteropentamers formed by α and β subunits at a 2:3 stoichiometry (9, 10). *GLRA4* is a pseudogene (8). Compared with other members of the LGIC superfamily, the subunit diversity of GlyRs is rather moderate, but posttranscriptional modifications generate a broad diversity. Alternative splicing of the large TM3-TM4 loop in α1 subunits leads to two GlyR α1 variants, α1Ins and α1ΔIns, which differ from each other in the presence or absence of an eight-amino acid insert (SPMLNLFQ), respectively (11). Likewise, two α3 variants, α3K and α3L, are generated by alternative splicing of GlyR α3 exon 8A (TEAFALEKFYRFSDT) located in the TM3-TM4 loop (12). For GlyR α2, alternative splicing of exon 3 generates two different receptor variants that differ by two amino acids (α2A (IA) and α2B (VT)) in the extracellular ligand binding domain (13).

To investigate GlyRs on a splice-specific level, detailed information about functional properties of each channel variant is needed. The electrophysiological properties of GlyR channels have been studied in various overexpression systems, including HEK293 cells and *Xenopus laevis* oocytes. Most likely due to the different cellular expression systems and cellular intrinsic signaling profiles, the apparent glycine affinity of the different homo- and heteromeric channel variants, for example, varies largely between 10 and 300 μM (8, 14–18). Hence, a study that compares all the GlyR variants in the same cellular context and using the same experimental setup is required to provide unambiguous information about the functional properties of different GlyR isoforms. A hallmark of all LGICs, including GlyRs, is the desensitization of currents in the continuous presence of a ligand, a mechanism that assures and shapes fast synaptic transmission (19). GlyR desensitization is a complex process that involves slow and fast decay components (1). Compared with the closely related GABA type A receptors ($GABA_AR$), GlyRs desensitize relatively slowly (0.5–11 s) (1, 12, 18). Here again,

* This work was supported by Bundesministerium für Bildung und Forschung (BMBF) Grant Era-Net NEURON II CIPRESS (to J. C. M.), Helmholtz Association Grant VH-NG-246 (to J. C. M.), and Deutsche Forschungsgemeinschaft (DFG) Priority Programme SPP 1784 ME2075/7-1 (to J. C. M.). The authors declare that they have no conflicts of interest with the contents of the article.

[1] Present address: Dept. of Biochemistry, University of Zurich, Winterthurerstr. 190, 8057 Zurich, Switzerland.

[2] Both authors contributed equally to this work.

[3] To whom correspondence may be addressed. Tel.: 49-531-391-3254; E-mail: jochen.meier@tu-braunschweig.de.

[4] To whom correspondence may be addressed. Tel.: 49-30-9406-3267; E-mail: marcus.semtner@mdc-berlin.de.

[5] The abbreviations used are: GlyR, glycine receptor; LGIC, ligand-gated ion channel; TM, transmembrane domain; IV, current-voltage; TRP, transient receptor potential; DIV, day(s) *in vitro*; WT, wildtype.

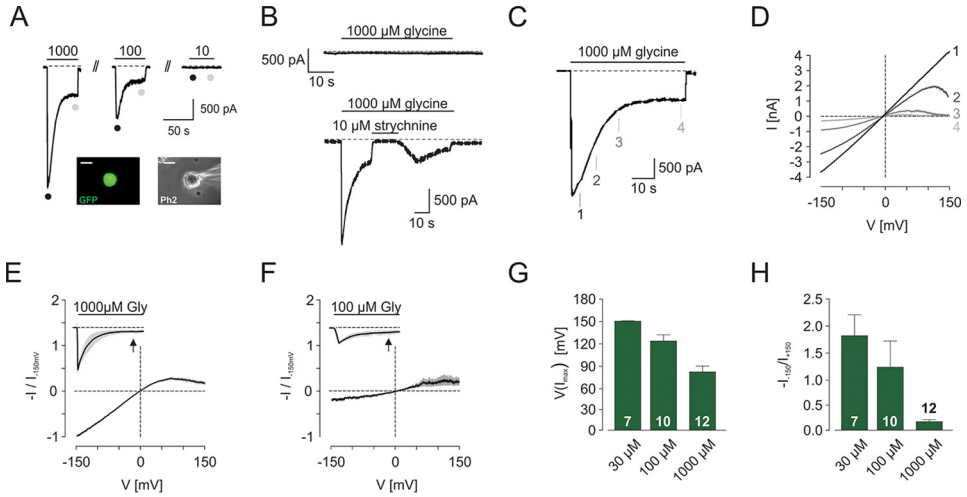

FIGURE 1. **Properties of glycine-evoked currents through GlyR α3L.** *A*, time course of currents at −50 mV evoked by 1000 μM (*left*), 100 μM (*middle*), and 10 μM (*right*) glycine in a whole-cell patch clamp experiment on a HEK293T cell transiently transfected with GlyR α3L. *Inset* images illustrate the recorded cell under fluorescence (GFP) and transmission (phase-contrast) illumination. *Scale bar*, 20 μm. *B*, non-transfected HEK293T cells did not respond to glycine application (*top*). Application of 10 μM strychnine reversibly blocked glycine-evoked currents in HEK293T cells transfected with GlyR α3L cDNA (*bottom*). *C*, expanded view of a GlyR α3L response to 1000 μM glycine. IV relationships at the indicated time points (*1–4*) are shown in *D*. *D*, IV relationships of homomeric GlyR α3L channels during current desensitization in response to 1000 μM glycine. Note that the IV relationships at peak are linear and become inwardly rectifying upon desensitization. *E*, averaged IV relationships of homomeric GlyR α3L channels upon desensitization and in response to 1000 μM glycine ($n = 12$). All IV relationships were normalized to the currents at −150 mV before merging. *F*, averaged IV relationships of homomeric GlyR α3L channels upon desensitization and in response to 100 μM glycine ($n = 10$). All IV relationships were normalized to the currents at −150 mV before merging and to the peak currents of responses at 1000 μM glycine after merging. *G*, summary of the potentials at which the maximal IV outward currents were determined ($V(I_{max})$), for currents evoked with 30, 100, and 1000 μM glycine. *H*, summary of the rectification index ($-I_{-150\ mV}/I_{+150\ mV}$) for currents through GlyR α3L homomers evoked with 30, 100, and 1000 μM glycine. *Error bars*, S.E.

time course and decay half time of desensitization underlie large cell-to-cell variability (20) due to many different parameters that may influence the kinetics, such as ligand concentration (16), the phosphorylation state of the intracellular TM3-TM4 loop (16, 20), or the membrane potential (1, 21, 22). GlyR are basically selective for Cl^- but also permeable to other anions and even to cations (23–28). Due to anomalous mole fraction effects on ion conductance, it has further been suggested that GlyRs are multi-ion channels with at least two ion binding sites in the channel pore (23, 24). The GlyR pore is formed by the TM2 helices from five channel-forming GlyR subunits. The narrowest point within the pore is located at the intracellular pore mouth and formed by the 2′-Pro and 9′-Leu residues within TM2 (29). Interestingly, amino acids from this region are involved not only in selectivity of GlyR to Cl^-, but also in determining its desensitization kinetics (18).

A current-voltage (IV) relationship characterizes and identifies an ion channel. Characteristic IV relationships were identified for many homo- and heteromeric ion channels, including members of the transient receptor potential (TRP) channel family (30, 31). However, in the case of GlyRs, detailed information about isoform-specific characteristics of IV relationships is not available, especially for α2- and α3-containing GlyRs that are involved in neuropathic pain, temporal lobe epilepsy, and autism spectrum disorder (3–6). Here, using the same (HEK293T) cellular expression system and the same experimental setup, we reveal essential information about characteristic IV relations of recombinant homomeric GlyR α2 and α3 channels. The results show that, upon receptor desensitization, the IV relationship switches from a linear behavior to an inwardly rectifying shape, in contrast to homomeric GlyR α1 or heteromeric GlyR α2/β or α3/β channels, where IV relationships remain linear. Furthermore, GlyR α2 and α3 IV rectification is dependent on a single amino acid at the inner pore mouth and closely linked to Cl^- permeation. This characteristic electrophysiological IV signature of homomeric GlyR α2 and α3 channels was also found in primary hippocampal neurons with preponderant GlyR α2 protein expression. Thus, our study not only provides useful information about the physiomolecular signature of GlyR channels and their identification in native cells but also may help in understanding the complex nature of maladaptive forms of neuronal plasticity in neuropathic pain, autism spectrum disorder, and temporal lobe epilepsy.

Results

Current-Voltage Relationships of Desensitized GlyR α3L Are Inwardly Rectifying—The electrophysiological properties of GlyR α3L were investigated in whole-cell patch clamp recordings on HEK293T cells transiently transfected with the cDNA of the receptor subunit. In agreement with previous publications, application of glycine elicited inward currents at −50 mV in a concentration-dependent manner (Fig. 1*A*). The time courses of glycine-evoked currents were characteristic in terms of a fast increase that was followed by a slow decline toward a steady state level, which is referred to as receptor desensitization. Note that although considered as inward current by convention, the Cl^- flux through GlyR α3L at −50 mV is actually directed outwardly. When glycine was removed from the bath solution, currents returned to baseline levels. The specificity of glycine-induced currents through GlyR α3L was further confirmed by application of the competitive antagonist strychnine (10 μM), which completely and reversibly blocked GlyR α3L

TABLE 1

Electrophysiological properties of GlyR channels at −50 mV

$I_{1000\ gly,\ peak}$, average amplitudes of peak currents through the indicated GlyR channels in whole-cell patch clamp recordings at −50 mV evoked by 1000 μM glycine. $EC_{50,\ peak}$ and $n_{H,\ peak}$, EC_{50} values and Hill coefficients of peak currents through the indicated GlyR channels in whole-cell patch clamp recordings at −50 mV. $\tau_{1000\ gly}$, averaged time constants of decay of currents through the indicated GlyR channels evoked by 1000 μM glycine. Values were determined by a monoexponential fit of the time courses at −50 mV. $I_{1000\ gly,\ desens.}$, Average amplitudes of peak currents through the indicated GlyR channels in whole-cell patch clamp recordings at −50 mV evoked by 1000 μM glycine. $EC_{50,\ desens.}$ and $n_{H,\ desens.}$, EC_{50} values and Hill coefficients of desensitized currents through the indicated GlyR channels in whole-cell patch clamp recordings at −50 mV. Current amplitudes were extracted from the time courses at −50 mV 25–35 s after glycine application. Numbers in parentheses indicate the number of experiments (*n*).

GlyR	$I_{1000\ gly,\ peak}$	$EC_{50,\ peak}$	$n_{H,\ peak}$	$\tau_{1000\ gly}$	$I_{1000\ gly,\ desens.}$	$EC_{50,\ desens.}$	$n_{H,\ desens.}$
	pA	μM		*s*	*pA*	μM	
α1ΔINS	−4352 ± 691 (9)	55.3 ± 8.5 (7–9)	1.2 ± 0.2 (7–9)	8.3 ± 2.5 (8)	−821 ± 121 (9)	36.9 ± 9.0 (7–9)	0.8 ± 0.2 (7–9)
α1INS	−5782 ± 561 (6)	65.4 ± 4.1 (4–6)	1.8 ± 0.2 (4–6)	6.6 ± 2.0 (5)	−1328 ± 114 (6)	30.3 ± 4.6 (4–6)	1.8 ± 0.5 (4–6)
α2A	−3741 ± 506 (12)	70.0 ± 1.8 (5–12)	2.1 ± 0.1 (5–12)	6.3 ± 1.0 (9)	−921 ± 120 (12)	35.8 ± 0.2 (5–12)	1.7 ± 0.0 (5–12)
α2B	−1998 ± 357 (11)	22.4 ± 1.6 (10–11)	1.6 ± 0.2 (10–11)	10.1 ± 1.8 (8)	−578 ± 106 (11)	43.6 ± 18.1 (10–11)	0.8 ± 0.3 (10–11)
α2Aβ	−3255 ± 722 (6)	155.0 ± 12.9 (4–6)	2.2 ± 0.4 (4–6)	7.0 ± 0.8 (6)	−755 ± 185 (6)	146.6 ± 37.5 (4–6)	1.5 ± 0.5 (4–6)
α2Bβ	−3796 ± 338 (5)	55.3 ± 8.5 (4–5)	1.2 ± 0.2 (4–5)	7.1 ± 1.8 (4)	−896 ± 162 (5)	36.9 ± 9.0 (4–5)	0.8 ± 0.2 (4–5)
α3K	−3006 ± 373 (14)	69.2 ± 4.7 (12–14)	1.4 ± 0.1 (12–14)	6.9 ± 1.1 (10)	−675 ± 100 (14)	66.2 ± 11.2 (12–14)	1.1 ± 0.2 (12–14)
α3L	−4086 ± 572 (23)	94.6 ± 0.5 (5–23)	2.3 ± 0.0 (5–23)	5.3 ± 1.1 (13)	−412 ± 76 (23)	40.0 ± 6.3 (5–23)	1.5 ± 0.3 (5–23)
α3Kβ	−3055 ± 457 (10)	118.4 ± 8.2 (6–10)	1.6 ± 0.2 (6–10)	5.3 ± 0.8 (10)	−463 ± 57 (10)	41.4 ± 3.1 (6–10)	2.8 ± 0.5 (6–10)
α3Lβ	−1642 ± 333 (8)	138.1 ± 15.6 (6–9)	1.7 ± 0.2 (6–9)	4.8 ± 1.1 (7)	−228 ± 57 (8)	57.5 ± 2.7 (6–9)	1.4 ± 0.1 (6–9)
$α3K^{A254G}$	−3175 ± 583 (14)	123.7 ± 11.5 (12–14)	1.7 ± 0.3 (12–14)	7.1 ± 2.3 (5)	−740 ± 104 (14)	85.1 ± 2.5 (12–14)	1.6 ± 0.1 (12–14)
$α3L^{A254G}$	−3344 ± 261 (20)	177.6 ± 29.0 (14–20)	2.5 ± 0.7 (14–20)	5.4 ± 0.7 (11)	−814 ± 51 (20)	113.6 ± 1.6 (14–20)	2.2 ± 0.1 (14–20)

responses to 1000 μM glycine (Fig. 1*B*, *bottom*). Non-transfected HEK293T cells did not respond to glycine (Fig. 1*B*, *top*).

IV relationships of GlyR α3L were determined at different time points of receptor activation by applying voltage ramps ranging from −150 to +150 mV (600 ms) every 5 s. As expected for a Cl^- channel, each IV relationship of GlyR α3L reversed close to the Nernst potential for Cl^- (−2.3 mV). Instantly after glycine administration, IV relationships of GlyR α3L were linear (Fig. 1, *C* and *D*) but, interestingly, became inwardly rectifying upon desensitization. To quantify this rectification, we analyzed IV relationships obtained 25–30 s after glycine application, a time point at which homomeric GlyR α3L channels were in a steady state because the time constant of desensitization was 5.3 ± 1.1 s ($n = 13$; monoexponential fit of time courses at −50 mV; see Table 1). The following parameters were extracted from these IVs: $-I_{+150\ mV}/I_{-150\ mV}$, which is a measure of the extent of IV rectification, and $V(I_{max})$, which gives the membrane potential at which the outward currents start to decline. Thus, a channel displaying a perfectly linear IV relationship (reversing at 0 mV), which exerts no rectification and no decline in conductance at positive potentials, had parameters of $-I_{+150\ mV}/I_{-150\ mV} = 1$ and $V(I_{max}) = 150$ mV. For desensitized GlyR α3L, $-I_{+150\ mV}/I_{-150\ mV}$ was 0.17 ± 0.04 ($n = 12$), and $V(I_{max})$ was 80.9 ± 8.2 mV ($n = 12$), indicating that the outward currents at +150 mV were nearly 7 times smaller than the inward currents at −150 mV and that this voltage-dependent decrease in conductance started at around +75 mV (Fig. 1*D* and Table 2). Interestingly, after submaximal activation of GlyR α3L with only 30 or 100 μM glycine, the IV inward rectification and the decline of conductance at positive potentials disappeared, and the IV relationships were rather linear (Fig. 1, *E–H*).

Determinants of GlyR α3L Rectification—We investigated whether an open channel block by intracellular Mg^{2+} or Ca^{2+} could be responsible for the reduced conductance of GlyR α3L at positive membrane potentials. A similar mechanism has been elucidated for other ion channels *e.g.* inward rectifier potassium channels (K_{ir}), where inward rectification depends on a highly voltage-dependent block by intracellular Mg^{2+} and organic polyamines (32–34). However, in the case of GlyR α3L, there was no change in the shape of the IV relationships when using Ca^{2+}- and Mg^{2+}-free pipette solutions containing 10 mM HEDTA (Fig. 2, *A* and *C*). Consequently, rectification ($-I_{+150\ mV}/I_{-150\ mV} = 0.21 \pm 0.10$, $n = 4$; $p = 0.5899$) and $V(I_{max})$ (79.9 ± 23.5 mV, $n = 4$; $p = 0.9591$) were similar to those in the experiments with standard pipette solution, indicating that an open channel block by intracellular divalent cations is unlikely to be responsible for the inward rectification.

To study the mechanisms of GlyR α3L rectification further, we considered the possibility that Cl^- permeation through GlyR α3L is limited at positive potentials. To address this option, we performed recordings on GlyR α3L using low intracellular Cl^- concentrations and applied 1000 μM glycine. As shown in Fig. 2, *B* and *C*, inward rectification was still present under these conditions; however, $V(I_{max})$ (28.1 ± 1.1 mV, $n = 5$) was strongly shifted toward more negative potentials. Intriguingly, when compared with high Cl^- pipette solutions, the shift of $V(I_{max})$ was similar to the shift of the reversal potential (−42.0 ± 2.1 mV, $n = 5$; Fig. 2*C*), indicating that the decrease in GlyR α3L conductance at positive membrane potentials is related to diminished Cl^- permeation at these membrane potentials.

IV Rectification Identifies Homomeric GlyRα2 and GlyRα3 Channels—We next studied the characteristics of different RNA splice variants of homomeric GlyR α1, GlyR α2, and GlyR α3 channels and compared their major properties with those of GlyR α3L. As shown in Fig. 3, each of the investigated isoforms responded to the application of glycine. All data on concentration-response curves and desensitization kinetics can be found in Table 1, and the parameters extracted from IV relationships are summarized in Table 2. Like GlyR α3L, the IV relationships of homomeric GlyR α2- and α3-containing channels were inwardly rectifying upon desensitization, whereas GlyR α1 channels displayed linear IV relationships. We also investigated GlyR α2/β and GlyR α3/β heteromeric channels. The β subunit was previously shown to influence not only the subcellular expression of GlyRs but also their biophysical properties. In our experiments, when comparing homomeric and heteromeric GlyR, the β subunit-containing channels generally tended to have lower affinities (EC_{50}) and smaller cooperativities (n_H) for

TABLE 2

Properties of GlyR IV relationships

V_{rev}, reversal potential of the IV relationships of the indicated GlyR channels. $V(I_{max})$, membrane potential of the maximum outward current in the IV. $-I_{+150\ mV}/I_{-150mV}$, currents at +150 mV normalized to currents at −150 mV. Numbers in parentheses indicate the number of experiments (*n*). For each data set, significant differences against linearity were calculated by a two-tailed *t* test of the data against $V(I_{max})$ = 150 mV and $-I_{+150\ mV}/I_{-150mV}$ = 1. ND, not determined; NS, not significant; *, $p < 0.05$; **, $p < 0.01$; ***, $p < 0.001$.

	Intracellular condition	V_{rev}	$V(I_{max})$	$-I_{+150\ mV}/I_{-150\ mV}$
		mV	*mV*	
HEK293				
α1ΔINS	Standard	−3.5 ± 1.7 (4)	138.3 ± 11.7 (4)^{NS}	0.72 ± 0.16 (4)^{NS}
α1INS	Standard	0.2 ± 0.8 (6)	150.0 ± 0.0 (6)^{NS}	0.93 ± 0.08 (6)^{NS}
α2A	Standard	−5.3 ± 1.5 (5)	122.9 ± 14.0 (5)^{NS}	0.51 ± 0.14 (5)*
α2B	Standard	−1.9 ± 1.6 (5)	118.0 ± 11.9 (5)^{NS}	0.47 ± 0.13 (5)*
α2Aβ	Standard	−0.2 ± 0.8 (6)	150 ± 0.0 (6)^{NS}	0.62 ± 0.07 (6)**
α2Bβ	Standard	−0.1 ± 0.4 (5)	144.9 ± 5.1 (5)^{NS}	0.725 ± 0.15 (5)^{NS}
α3K	Standard	−2.3 ± 1.0 (9)	105.3 ± 10.1 (9)**	0.41 ± 0.08 (9)***
α3L	Standard	0.2 ± 0.5 (12)	80.9 ± 8.2 (12)***	0.17 ± 0.04 (12)***
α3L, 30 μM Gly	Standard	0.9 ± 2.3 (7)	149.6 ± 0.4 (7)^{NS}	1.82 ± 0.38 (7)***
α3L, 100 μM Gly	Standard	3.6 ± 0.3 (10)	122.3 ± 8.5 (10)**	1.17 ± 0.50 (10)^{NS}
α3L	$-Mg^{2+}/Ca^{2+}$	−3.1 ± 0.6 (4)	79.9 ± 23.5 (4)*	0.21 ± 0.10 (4)**
α3L	18 mM Cl^-	−42.0 ± 2.1 (5)ND	28.1 ± 1.1 (5)ND	0.41 ± 0.04 (5)ND
α3Kβ	Standard	0.2 ± 0.6 (8)	144.9 ± 5.0 (8)^{NS}	0.59 ± 0.13 (8)**
α3Lβ	Standard	0.6 ± 0.3 (8)	146.6 ± 2.6 (8)^{NS}	0.37 ± 0.07 (8)***
α3K-A254G	Standard	−2.8 ± 1.1 (6)	150.0 ± 0.0 (6)^{NS}	0.98 ± 0.08 (6)^{NS}
α3L-A254G	Standard	−3.6 ± 1.2 (12)	114.4 ± 8.6 (12)**	0.57 ± 0.09 (12)***
HC neuron				
DIV 2–4	Standard	0.8 ± 1.7 (8)	91.8 ± 9.8 (8)***	0.19 ± 0.03 (8)***
DIV 15–25	Standard	2.4 ± 2.5 (9)	132.8 ± 13.1 (9)^{NS}	0.29 ± 0.08 (9)***

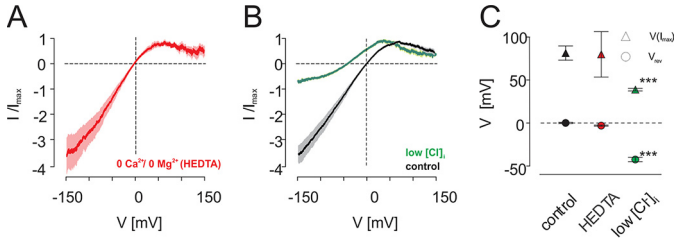

FIGURE 2. **GlyR α3L inward rectification is linked to Cl^- permeation.** *A*, averaged IV relationships of GlyR α3L upon desensitization and in response to 1000 μM glycine ($n = 4$). IV relationships were normalized to the maximum outward current. Experiments were done using a Ca^{2+}/Mg^{2+}-free pipette solution containing 10 mM HEDTA. *B*, averaged IV relationships of GlyR α3L upon desensitization and in response to 1000 μM glycine. IV relationships were normalized to the maximum outward current. Experiments were performed with the standard pipette solution (*black*, $n = 12$) and with a pipette solution containing only 18 mM Cl^- (*green*, $n = 5$). *C*, statistical analysis of the reversal potentials (V_{rev}, *circles*) and the potentials at which the maximal outward currents were determined ($V(I_{max})$, *triangles*) at the conditions shown in *A* and *B*. Note that $V(I_{max})$ was dependent on the Cl^- driving force and was not changed by intracellular Ca^{2+} or Mg^{2+}. *Error bars*, S.E.

glycine, which is in agreement with previous observations (9). Furthermore, β subunit-containing GlyRs desensitized more slowly compared with corresponding homomeric receptor channels. Most interestingly, although inward rectification remained at substantial levels, the IV relationships of GlyR α2/β and GlyR α3/β heteromers were much more linear compared with their homomeric counterparts (Fig. 3, *B* and *C*, and Table 2).

GlyR Pore Structure Is Closely Linked to IV Rectification—To identify the molecular determinants of GlyR inward rectification, we compared the amino acid sequences of the pore-lining (TM2) regions of rodent GlyR α1–3 (Fig. 4*A*). Intriguingly, the pore regions are almost completely identical, and only at position 254, GlyR α1 subunits carry a glycine, whereas an alanine residue is present in GlyR α2 and α3 subunits. Amino acid substitution of glycine for alanine at position 254 in GlyR α3 led indeed to a strongly diminished inward rectification of desensitized currents through both GlyR α3 splice isoforms (Fig. 4*C*), indicating that alanine at position 254 is a major determinant of this characteristic. The recently published cryo-EM structure of GlyR α1 (29) reveals that Gly^{254} in GlyR α1 is located at the inner mouth of the channel pore and directed toward the permeation pathway (Fig. 4*B*, shown in *red*). We generated a structure homology model (35) of GlyR α3 based on GlyR α1. However, the side chain of alanine in this structure model was not directed toward the channel pore, indicating that permeating ions are presumably not sterically hindered by the additional methyl group in GlyR α3 channels. We therefore suggest minimal differences in TM2 positioning relative to the channel pore of GlyR α1 and α3 as a possible reason for the differences in the IV curves. Notably, GlyR β subunits also differ from GlyR α3 at position 254 and hold a proline instead of alanine (Fig. 4*A*). The fact that the IV relationships of β subunit-containing GlyR channels were not rectifying further supports our hypothesis that is based on mutagenesis and tertiary structure analysis.

Functional Determination of Somatic GlyR Subunit Composition in Hippocampal Neurons—We finally asked whether the particular biophysical characteristics of GlyR α1 *versus* α2 and α3 can be used as an electrophysiological signature or fingerprint of the neuronal endogenous GlyR subunit composition. It was recently shown that the GlyR β subunit is expressed as mRNA, not as protein, in mouse hippocampal neurons (36). We performed patch clamp experiments on rat primary hippocampal neurons. In immature neurons at DIV 2–4, IV relationships of 1000 μM glycine-evoked currents clearly had an inwardly rectifying shape that resembled mostly those of transiently expressed GlyR α2 or α3 homomeric channels in HEK293T cells (Fig. 5*B*; compare with Fig. 3*C*). Messenger RNA coding for GlyR α3 was detected in primary hippocampal neurons, although at rather low levels compared with those corresponding to GlyR α2 and GlyR β coding transcripts (Fig. 5*A*). The same holds true for more mature hippocampal neurons at DIV 15–25. However, there were significant differences in the shape of their IV relationships, which were much more

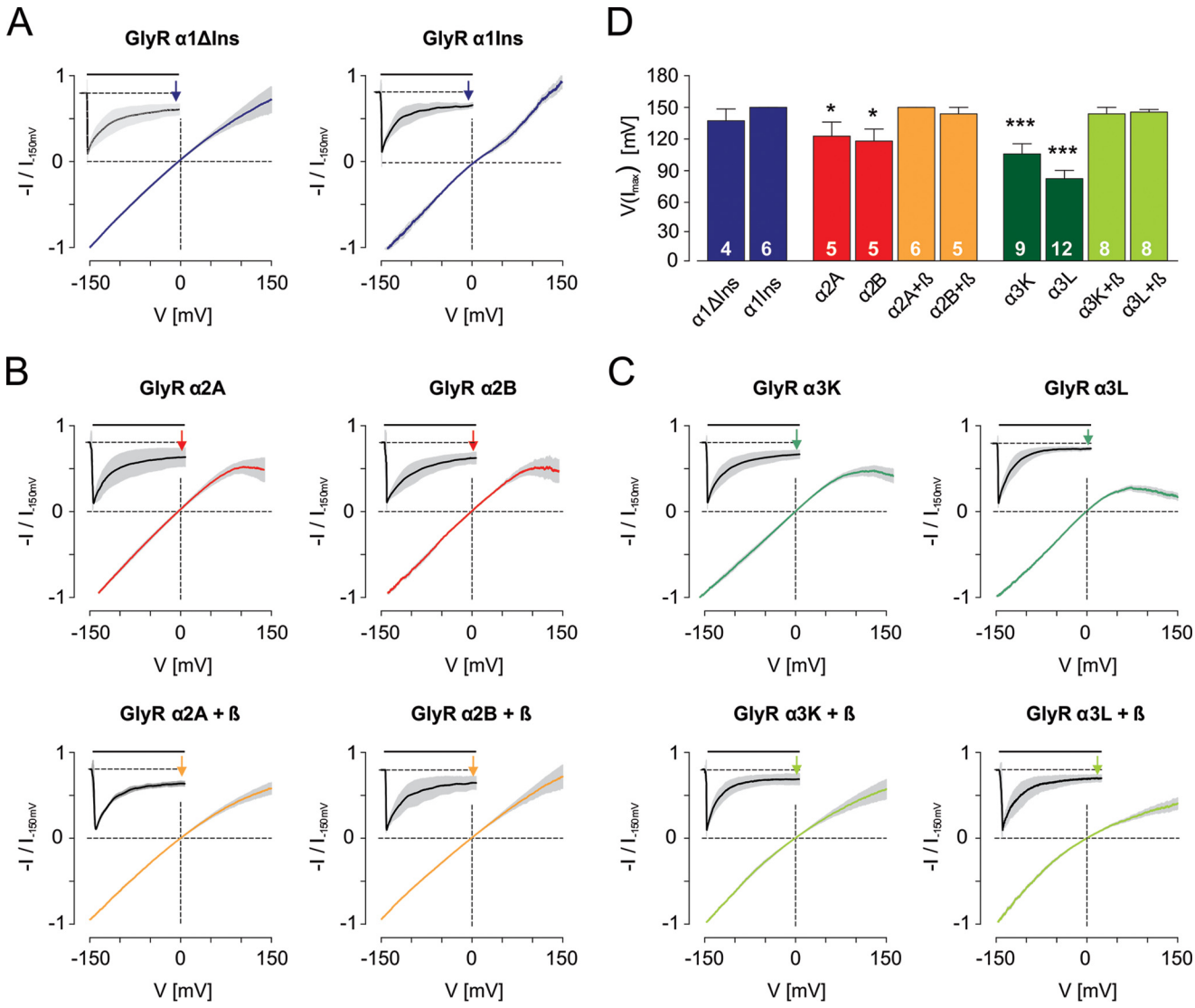

FIGURE 3. **IV relationships of desensitized currents through GlyR channels.** *A–C*, averaged IV relationships of homomeric GlyR α1ΔIns (*A*, *left*) and GlyR α1Ins (*A*, *right*), GlyR α2A (*B*, *top left*) and GlyR α2B (*B*, *top right*), and GlyR α3K (*C*, *top left*) and GlyR α3L (*C*, *top right*) as well as heteromeric GlyR α2A/β (*B*, *bottom left*) and GlyR α2B/β (*B*, *bottom right*) and GlyR α3K/β (*C*, *bottom left*) and GlyR α3L/β (*C*, *bottom right*) channels upon desensitization and in response to 1000 μM glycine. IV relationships were normalized to the currents at −150 mV. *Insets*, averaged and normalized time courses at −50 mV from 2 s before to 30 s after the start of glycine application. *D*, statistical analysis of the potentials at which the maximal outward currents were determined ($V(I_{max})$). The *color code* is similar to that in *A–C*. Note that only homomeric GlyR α2 and GlyR α3 channels display pronounced inward rectification. *Error bars*, S.E.

linear than those from immature neurons but still displayed substantial inward rectification (Fig. 5, *B–E*).

Discussion

GlyRs are ligand-gated chloride channels that contribute to synaptic signal transmission in the mammalian CNS. Currently, there are inconsistent data regarding biophysical properties of GlyRs due to heterogeneous heterologous expression systems. Here, we comparatively investigated the properties of glycine-evoked currents through recombinant GlyR channels using GlyR α1–3 splice variants as well as heteromeric GlyR α/β channels in the same heterologous expression system and using the same experimental setup. We studied glycine sensitivities after receptor desensitization and IV relationships of GlyR channels with different subunit compositions. The results reveal intriguing differences between homomeric GlyR α2/3 and α1 channels currents during desensitization with regard to IV rectification upon pronounced depolarization. Furthermore, our study identifies a single critical amino acid in transmembrane domain 2 that is responsible for voltage-dependent rectification of glycine-dependent currents in the desensitized state, which renders GlyR α1 and heteromeric GlyR α/β channels insensitive to voltage-dependent rectification of transmembrane chloride conductance during receptor desensitization. Apparent glycine sensitivity was higher in the desensitized state of GlyR α3L channels, and the Hill coefficient tended to be lower compared with the instantaneous responses to 1000 μM glycine. Interestingly, this was the case not only for GlyR α3L channels but also for all other homomeric GlyR channels (except GlyR α2B). Although the EC_{50} and n_H values derived from concentration-response curves alone are not suited to directly distinguish between agonist binding and channel gating, due to the uncertain occupancy and cooperativity of the glycine binding sites as well as possible structural and kinetic

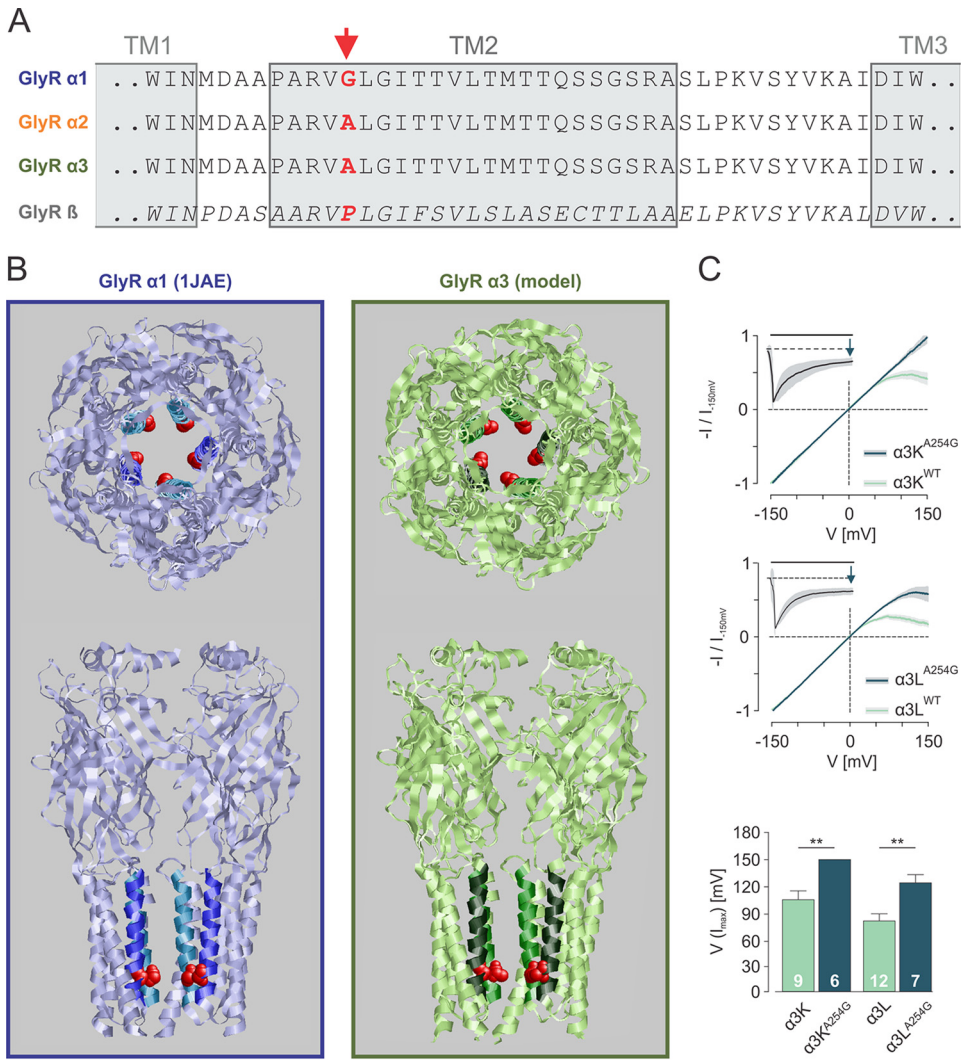

FIGURE 4. **An alanine residue within the GlyRα3 pore is important for inward rectification.** *A*, sequence comparison of the pore-lining regions of GlyR α1, GlyR α2, GlyR α3, and GlyR β subunits (starting from position 243). Note that the sequences of all α subunits are completely identical with the exception of one alanine/glycine at position 254. *B*, *left*, front (*bottom*) and top (*top*) view on homomeric GlyR α1 in the glycine-bound state (Protein Data Bank entry 1JAE). Gly^{254} is located at the inner pore mouth and directed toward the channel pore. *Right*, structure homology model of a homomeric GlyR α3 channel. The side chain of Ala^{254} is not directed toward the channel pore. *C*, averaged IV relationships of A254G mutants of GlyR α3K (*top*) and GlyR α3L (*middle*) upon desensitization and in response to 1000 μM glycine. IV relationships were normalized to the currents at −150 mV. IV relationships of GlyR $\alpha3K^{wt}$ and GlyR $\alpha3L^{wt}$ are illustrated for comparison. Experiments were performed with the standard pipette solution. *Insets*, averaged and normalized time courses at −50 mV from 2 s before to 30 s after glycine application. *Bottom*, statistical analysis of $V(I_{max})$. Inward rectification of the A254G mutants was significantly reduced in comparison with WT. *Error bars*, S.E.

differences in gating (37, 38), our data suggest that the amino acid sequence homology between the different GlyR α variants gives rise to similar desensitization properties at −50 mV. Indeed, the desensitization kinetics expressed as τ values were consistent between 5 and 10 s for each of the investigated homomeric GlyR α channels. However, these data are not in good agreement with previous studies that reported that splicing of the long insert into GlyR α3 mRNA impacts on desensitization kinetics (12, 39–41). Notably, desensitization of GlyR channels may be highly variable (20, 41) and influenced by many parameters, such as receptor density (42), membrane potential (43), intracellular and extracellular pH (44, 45), ion concentration (46, 47), the membrane lipid composition, and phosphorylation of the intracellular TM3-TM4 domain or the *N*-glycosylation of the receptor N terminus (20). Technical features, such as slow or fast ligand application or the ligand concentration (16, 48), duration of ligand administration, or the recording mode may also account for these differences. Co-expression of the GlyR β subunit did not change Hill coefficients of glycine-response curves and decay kinetics of GlyR α2- and GlyR α3-containing channels, but the sensitivity of heteromeric channels was consistently increased by a factor of approximately 2 in comparison with the respective homomeric GlyR α2/3 variants, which is a new finding compared with recent publications that did not report such a tendency for α2-containing or α3-containing GlyRs (49–51). Differences in the binding affinities of glycine between the sites formed by α/α or the α/β surfaces were previously resolved (52), possibly explaining these differences from previous studies.

We also investigated IV relationships of GlyR channels with different subunit compositions. The IV relationship of an ion channel can be regarded as a signature. It is an important

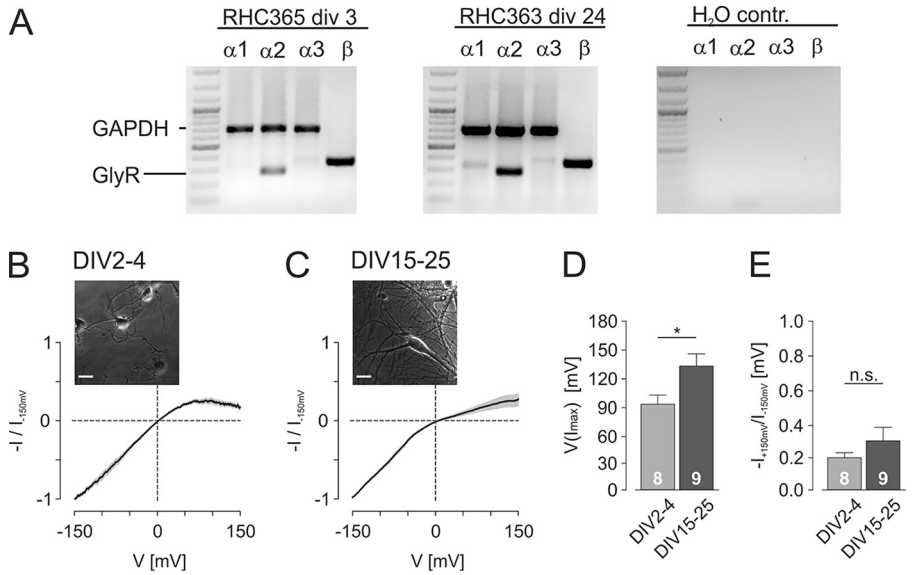

FIGURE 5. **Functional GlyR subunit expression in hippocampal neurons.** *A*, PCR of cDNA from cultured hippocampal neurons at DIV 3 or DIV 24 using specific primers for GlyR α1, GlyR α2, GlyR α3, and GlyR β cDNAs. GAPDH was tested in parallel in PCRs for GlyR α1, GlyR α2, and GlyR α3. Note that mRNA levels of GlyR α2 and GlyR β are more pronounced than those of GlyR α1 and GlyR α3 at both time points. *B* and *C*, averaged IV relationships of DIV 2–4 neurons upon desensitization and in response to 1000 μM glycine. Note that IVs were determined by subtraction of currents in the presence and absence of glycine. IV relationships were normalized to the currents at −150 mV. Experiments were performed with the same pipette solution as used in HEK293T cells. *Insets*, representative transmission light (Ph2) images from a neuron at DIV 3 (*B*) or at DIV 24 (*C*). *Scale bar*, 20 μm. *D*, summary of the potentials at which the maximal IV outward currents were determined ($V(I_{max})$) for currents evoked by 1000 μM glycine in DIV 2–4 and DIV 15–25 neurons. *E*, summary of the rectification index ($-I_{-150\ mV}/I_{+150\ mV}$) for currents evoked by 1000 μM glycine in DIV 2–4 and DIV 15–25 neurons. *Error bars*, S.E.

parameter to characterize and identify an ion channel's biophysical properties or the subunit composition *in vitro* and *in vivo*. For GlyR channels, few data are available with respect to their IV relations, although glycine-induced currents through these channels are known to be voltage-dependent (21, 48, 53). However, many studies on IV relations of native or recombinant GlyR α1-containing channels were performed using different cellular expression systems, including neurons, HEK cells, and *Xenopus* oocytes (23, 24, 54–56). In the present study, we describe for the first time IV relationships of homomeric and heteromeric GlyR channels over a wide voltage range from −150 to +150 mV using the same HEK293T cellular expression system. The finding that IV relations of homomeric GlyR α2 and α3 channels change from linear to inwardly rectifying upon desensitization might be indicative for the changes of the structural configuration of the agonist binding sites, channel pore, linker sequences, and intracellular domains, altogether leading to the apparent changes in conductance (37). However, our data show that GlyR α3 inward rectification depends to a large extent on ion permeation because inward rectification of GlyR α3L was observed with both symmetrical and asymmetrical Cl^- gradients, and the membrane potential of the onset of rectification ($V(I_{max})$) shifted to the same extent as the Nernst potential would predict. Thus, the inward rectification of desensitized GlyR α3L currents is not dependent on a given membrane potential but rather on a given chemical Cl^- gradient across the membrane. Interestingly, a three-site/four-barrier rate model was previously suggested for GlyR α1 (25), and rectification of the single channel conductance can be changed by point mutations of the amino acids that putatively contribute to the barriers within the channel pore (26). We have found that inward rectification of a GlyR α3L mutant, A254G, was significantly reduced. Alanine at position 254 in the TM2 is located at the inner channel pore mouth of GlyR α3L and can be considered analogous to Gly^{254} in GlyR α1, where it is located at position 2′ in the pore-forming TM2 transmembrane helix (26, 29). Substituting glycine with alanine actually deletes only a methyl group but does not introduce or delete charged or polar residues in a protein. It is therefore likely that, structurally, either the pore diameter is affected or the general positioning of TM2 is changed by the A254G mutation in GlyR α3L. However, our data do not favor one of these two possibilities, and the protein homology structure model of GlyR α3 (see Fig. 4) predicts that the methyl group of Ala^{254} is not directly displayed toward the pore. Rather, mutational studies on GlyR α1 (57) have suggested that ion permeation is sterically regulated at the inner pore mouth between positions −3′ and +2′ relative to TM2. It is furthermore accepted that the narrowest point in the GlyR pore is located at the inner mouth (29, 58). Our results therefore suggest that the inwardly rectifying IV relationship of desensitized GlyR α3 channels is most likely determined by an asymmetrical energy barrier for Cl^- permeation. Interestingly, gating and permeation of LGICs are closely linked, and desensitization was recently shown to be regulated by interactions between the TM2 and TM3 segments, affecting the lumen of the channel pores close to the intracellular side (18). Although position 254 (Gly^{254} in α1, Ala^{254} in α2 and α3) was not directly investigated in that study, it is close to the other positions (*e.g.* Gly^{256} in α1) (18) that are involved in TM2-TM3 coupling and receptor desensitization. Thus, Ala^{254} in GlyR α2 and α3 homomeric channels determines rectification of the IV relationship in the desensitized state, which is most likely due to an asymmetrical energy barrier for Cl^- permeation. Our study also showed that inward rectification only occurs with homomeric

GlyR α2 and α3 channels, consistent with the presence of an alanine at position 254. In contrast, IV relationships of homomeric GlyR α1 channels or heteromeric GlyR α2/β or GlyR α3/β channels were rather linear in the desensitized state. The inwardly rectifying IV relationship can therefore be regarded as a signature of homomeric GlyR α2 or α3 channels, which is useful for the discrimination of these GlyR channels from homomeric GlyR α1 or heteromeric GlyR α2 and α3 channels that contain the β subunit. Indeed, primary hippocampal neurons investigated at DIV 2–25 were shown here to display GlyR responses with rather inwardly rectifying IV relationships upon desensitization, suggesting that homomeric GlyR α2 and/or α3 channels were expressed at these developmental states. Our RT-PCR analysis provides evidence that supports this conclusion because GlyR α2 was preponderantly expressed between DIV 3 and DIV 24 (Fig. 5*A*). The finding that mRNA coding for GlyR β was also detected actually also supports recent evidence for the lack of GlyR β protein expression in hippocampal neurons (36). Furthermore, these results indicate that the identified voltage-dependent rectification of homomeric GlyR α2/3 can be used as physio-molecular signature to identify these channels at the single cell level.

In vivo, GlyR α2 and α3 are expressed in different brain regions, including the neocortex and hippocampus, in both post- and presynaptic neuronal compartments (2, 4, 8, 59, 60). The intracellular chloride concentration of most mature neurons in the CNS is relatively low, shifting the onset of GlyR rectification in the physiological range of membrane potentials. Thus, postsynaptic plasma membrane homomeric GlyR α2 or GlyR α3 channels would restrain chloride conductance at depolarized membrane potentials (*e.g.* during a series of action potentials and resulting massive membrane depolarization) if glutamatergic synapses are active. However, at presynaptic terminals of glutamatergic synapses, homomeric GlyR α3L was shown to be expressed in presynaptic vesicles with the ligand-binding domain facing the lumen of vesicles (4). Because the vesicular membrane potential would be much more positive compared with the plasma membrane potential, ranging between +40 and +80 mV (61), voltage-dependent rectification of GlyR-dependent currents can be particularly relevant with regard to the loading of vesicles with neurotransmitters because it would contribute to increasing ΔpH. The glycine transporter GlyT1 is also expressed at glutamatergic terminals in the vesicular membrane (62), and vesicle loading with glutamate indeed depends on the vesicular chloride gradient (63). Thus, vesicular GlyRs would be permanently desensitized (due to GlyT1-dependent glycine fill) and restrain chloride-facilitated glutamate loading of presynaptic vesicles, due to voltage-dependent rectification.

Altogether, our study reveals that inward rectification of IV relationships of desensitized homomeric GlyR α2 and α3 is a physio-molecular signature of these channels and a peculiar biophysical property that restrains chloride conductance at depolarized membrane potentials or in compartments with a low chloride concentration, which can be particularly relevant for maladaptive forms of neuronal plasticity in neuropsychiatric disorders, such as autism (5), and epilepsy (3, 4).

Experimental Procedures

Molecular Biology—The clones coding for GlyR α1ΔIns, GlyR α1Ins, GlyR α2A, GlyR α2B, and GlyR β were described earlier (64). In these cases, EGFP (Clontech) was co-expressed. Cloning of GlyR $\alpha3K^{A254G}$ and GlyR $\alpha3L^{A254G}$ was performed using Fusion-PCR with oligonucleotides 5′-GGGTAGGCCT-GGGTATCACCACTGTACTTACGA-3′ and 5′-CCCAGGC-CTACCCGAGCCGGAGCTGCA-3′ followed by StuI restriction digest and self-ligation. IRES-EGFP (expression of GFP from an internal ribosome entry site) constructs containing GlyR α3K, GlyR α3L, GlyR $\alpha3K^{A254G}$, or GlyR $\alpha3L^{A254G}$ were generated by molecular subcloning. RNA was isolated from DIV 2–4 primary rat hippocampal neurons using TRIzol reagent (Invitrogen). cDNA was obtained by reverse transcription of 2 μg of RNA with an equimolar mixture of 3′-anchored poly(T) oligonucleotides (T18V, T15V, and T13V) and Superscript II (Invitrogen), according to the manufacturer's protocol. cDNA of DIV 2–4 primary rat hippocampal neurons was screened for expression of GlyR subunits using PCR and oligonucleotides specific to GlyR α1 (5′-CTGTTTGCCTGCTCTT-CGTGT-3′ and 5′-TGGGGAAACCGATGCGAGATA-3′), α2 (5′-CAGCAGTGAACTTTGTCTCC-3′ and 5′-GAAGGCCA-GTGGGAAGGCAG-3′), α3 (5′-GATGTTCAAACATGCAT-AATGCAAC-3′ and 5′-GCCCGGGATCCAGAACTCTG-3′), and β (5′-TGAGCAAGCAGATGGGAAAGG-3′ and 5′-TAA-CGTTGAAGAACAAGAAGCAG-3′). cDNA coding for the housekeeping gene *Gapdh* (glyceraldehyde 3-phosphate dehydrogenase) was amplified using GAPDH-specific primers (5′-CAGTATGACTCTACCCACGG-3′ and 5′-CTCAGTGTAG-CCCAGGATG-3′). The PCR protocol consisted of an initial denaturation step (2 min at 94 °C) followed by 35 cycles with 94 °C denaturation (1 min), 58 °C annealing temperature (1 min), and 72 °C elongation (1 min). PCR products were separated using agarose gel electrophoresis and visualized using ethidium bromide.

Cell Culture and Transfection—HEK293T cells were cultured in T75 culture flasks containing 10 ml of DMEM (catalog no. 41965-062, Gibco) supplemented with 4.5 g/liter glucose, 10% FCS (catalog no. 1050064, Life Technologies), and 1% penicillin/streptomycin (catalog no. 15140122, Life Technologies) at 37 °C and 5% CO_2 in a humidified incubator. Cell passaging was performed every 2–3 days at an average confluence of 80–90%. Two or 3 days before transfection, 300,000 HEK293T cells were seeded onto 35-mm culture dishes containing 1.5 ml of DMEM/FCS/penicillin/streptomycin to reach 90–100% confluence for transfection with FuGENE® HD transfection reagent (catalog no. 04 709 705 001, Roche Applied Science) according to the manufacturer's instructions. 1 μg of DNA was used per transfection. Co-transfection was performed using the following: α + β (0.3 + 0.7 μg), α + GFP (0.9 + 0.1 μg), and α + β + GFP (0.2 + 0.7 + 0.1 μg). For electrophysiological recordings, transfected HEK293T cells were seeded onto glass coverslips (diameter 13 mm) coated for 20–30 min with 0.1% polyornithin (poly-DL-ornithine hydrobromide, catalog no. P8638-100MG, Sigma). Cells were allowed to adhere for at least 2 h before electrophysiological recordings were carried out.

Hippocampal Cell Culture—All animals were killed according to the permit (LaGeSo, 0122/07) given by the Office for Health Protection and Technical Safety of the regional government of Berlin and in compliance with regulations laid down in the European Community Council Directive. Primary hippocampal neurons from E19 Wistar rats were prepared as described previously (65) and kept in B27- and 1% FCS-supplemented Neurobasal medium (66). The initial cell density was 68,000/cm^2.

Electrophysiology—A ListMedical amplifier, an ITC-18 interface, and Patchmaster software (HEKA, Lamprecht, Germany) were used for patch clamp recordings. Patch pipettes, made from borosilicate glass (Science Products, Hofheim, Germany), had resistances of 2–6 megaohms when filled with the intracellular solution containing 130 mM CsCl, 5 mM NaCl, 0.5 mM $CaCl_2$, 1 mM $MgCl_2$, 5 mM EGTA, and 30 mM HEPES, pH 7.2 (CsOH). The Ca^{2+}/Mg^{2+}-free pipette solution contained 130 mM CsCl, 5 mM NaCl, 10 mM HEDTA, and 30 mM HEPES, pH 7.2 (CsOH) The low-chloride pipette solution contained 10 mM CsCl, 120 mM $CsMeSO_4$, 5 mM NaCl, 0.5 mM $CaCl_2$, 1 mM $MgCl_2$, 5 mM EGTA, and 30 mM HEPES, pH 7.2 (CsOH). The standard extracellular solution (pH 7.4) contained 140 mM NaCl, 5 mM KCl, 1 mM $MgCl_2$, 2 mM $CaCl_2$, 10 mM HEPES-NaOH, and 10 mM glucose. All chemicals were obtained from Sigma. Cells were voltage-clamped at a potential of −50 mV. Series resistances (R_s), monitored by −5 mV voltage pulses (50 ms) applied every 5–10 s, were between 5 and 30 megaohms. IV relationships were obtained by voltage ramps ranging from −150 to +150 mV applied every 5–10 s. Data were acquired with a sampling frequency of 10 kHz after Bessel filtering at 2.8 kHz. All experiments were performed at room temperature (20–25 °C). Transfected cells were identified by the EGFP fluorescence (see "Molecular Biology"). Perfusion of the extracellular solutions was gravity-driven. A perfusion pencil with a 200-μm tip placed at a distance of 100–200 μM from the recorded cell was used to obtain relatively short wash-in/wash-out times (<1 s).

Data Analysis and Statistics—Offline analysis of the data was performed using IGOR Pro version 6.37 (WaveMetrics, Lake Oswego, OR). From each experiment and at each glycine concentration, we extracted the currents at −50 mV before glycine application (I_{bas}), at the peak response (during the first second of glycine application; I_{peak}) and after 25–35 s of continuous glycine presence in the bath (I_{desens}). I_{peak} and I_{desens} were corrected for I_{bas} before generating the concentration-response curves. EC_{50} and n_H values were determined by fitting the concentration-response curves (normalized to 1000 μM glycine) from each experiment with the Hill equation. The τ values of decay were calculated as the mean from the monoexponential fit of the decay of (1000 μM) glycine-evoked currents from each experiment. For the illustration of current decay, time courses at −50 mV were normalized to their peak responses during glycine application and then merged. IV relationships were generated from voltage ramps ranging from −150 to +150 mV applied every 5–10 s. For analysis, we extracted an IV that was recorded immediately before glycine and subtracted it from a given IV in the presence of glycine. The merged IVs shown in the present paper were derived by averaging all IVs from one and the same condition after normalization to either $I_{-150\ mV}$ or its maximum current. Reversal potentials (V_{rev}), potentials of the maximum current ($V(I_{max})$), and $-I_{+150\ mV}/I_{-150\ mV}$ values were determined from the IV relationships. V_{rev} and $V(I_{max})$ were corrected offline for liquid junction potentials using Patcher's Power Tools (Francisco Mendez and Frank Würriehausen, Göttingen, Germany). Calculated liquid junction potentials were +5.0 mV for the standard intracellular solution and the Ca^{2+}/Mg^{2+}-free intracellular solution and +11.0 mV for the low chloride pipette solution.

Author Contributions—C. R. and F. H. conducted most of the experiments and analyzed the results. M. S. and J. C. M. wrote most of the paper. A. W. cloned most of the cDNAs and generated the point mutations. M. S. and J. C. M. conceived the idea for the project.

Acknowledgments—We thank Anne Schäfer, Silke Dusatko, Maren Wendt, Andra Eisenmann, and Carola Bernert for excellent technical assistance and Dr. Oliver Daumke for fruitful discussions on the manuscript.

References

1. Legendre, P. (2001) The glycinergic inhibitory synapse. *Cell Mol. Life Sci.* **58,** 760–793
2. Lynch, J. W. (2009) Native glycine receptor subtypes and their physiological roles. *Neuropharmacology* **56,** 303–309
3. Çalişkan, G., Müller, I., Semtner, M., Winkelmann, A., Raza, A. S., Hollnagel, J. O., Rösler, A., Heinemann, U., Stork, O., and Meier, J. C. (2016) Identification of parvalbumin interneurons as cellular substrate of fear memory persistence. *Cereb. Cortex* **26,** 2325–2340
4. Winkelmann, A., Maggio, N., Eller, J., Caliskan, G., Semtner, M., Häussler, U., Jüttner, R., Dugladze, T., Smolinsky, B., Kowalczyk, S., Chronowska, E., Schwarz, G., Rathjen, F. G., Rechavi, G., Haas, C. A., *et al.* (2014) Changes in neural network homeostasis trigger neuropsychiatric symptoms. *J. Clin. Invest.* **124,** 696–711
5. Pilorge, M., Fassier, C., Le Corronc, H., Potey, A., Bai, J., De Gois, S., Delaby, E., Assouline, B., Guinchat, V., Devillard, F., Delorme, R., Nygren, G., Råstam, M., Meier, J. C., Otani, S., *et al.* (2016) Genetic and functional analyses demonstrate a role for abnormal glycinergic signaling in autism. *Mol. Psychiatry* **21,** 936–945
6. Harvey, R. J., Depner, U. B., Wassle, H., Ahmadi, S., Heindl, C., Reinold, H., Smart, T. G., Harvey, K., Schutz, B., Abo-Salem, O. M., Zimmer, A., Poisbeau, P., Welzl, H., Wolfer, D. P., Betz, H., *et al.* (2004) GlyR α3: an essential target for spinal PGE2-mediated inflammatory pain sensitization. *Science* **304,** 884–887
7. Breitinger, H. G., Villmann, C., Becker, K., and Becker, C. M. (2001) Opposing effects of molecular volume and charge at the hyperekplexia site α1 (P250) govern glycine receptor activation and desensitization. *J. Biol. Chem.* **276,** 29657–29663
8. Legendre, P., Förstera, B., Jüttner, R., and Meier, J. C. (2009) Glycine receptors caught between genome and proteome: functional implications of RNA editing and splicing. *Front. Mol. Neurosci.* **2,** 23
9. Grudzinska, J., Schemm, R., Haeger, S., Nicke, A., Schmalzing, G., Betz, H., and Laube, B. (2005) The β subunit determines the ligand binding properties of synaptic glycine receptors. *Neuron* **45,** 727–739
10. Webb, T. I., and Lynch, J. W. (2007) Molecular pharmacology of the glycine receptor chloride channel. *Curr. Pharm. Des.* **13,** 2350–2367
11. Malosio, M. L., Grenningloh, G., Kuhse, J., Schmieden, V., Schmitt, B., Prior, P., and Betz, H. (1991) Alternative splicing generates two variants of the α1 subunit of the inhibitory glycine receptor. *J. Biol. Chem.* **266,** 2048–2053
12. Nikolic, Z., Laube, B., Weber, R. G., Lichter, P., Kioschis, P., Poustka, A., Mülhardt, C., and Becker, C. M. (1998) The human glycine receptor subunit α3: Glra3 gene structure, chromosomal localization, and func-

tional characterization of alternative transcripts. *J. Biol. Chem.* **273,** 19708–19714
13. Kuhse, J., Kuryatov, A., Maulet, Y., Malosio, M. L., Schmieden, V., and Betz, H. (1991) Alternative splicing generates two isoforms of the α2 subunit of the inhibitory glycine receptor. *FEBS Lett.* **283,** 73–77
14. Breitinger, U., Breitinger, H. G., Bauer, F., Fahmy, K., Glockenhammer, D., and Becker, C. M. (2004) Conserved high affinity ligand binding and membrane association in the native and refolded extracellular domain of the human glycine receptor α1-subunit. *J. Biol. Chem.* **279,** 1627–1636
15. Breitinger, H. G., Villmann, C., Melzer, N., Rennert, J., Breitinger, U., Schwarzinger, S., and Becker, C. M. (2009) Novel regulatory site within the TM3-4 loop of human recombinant α3 glycine receptors determines channel gating and domain structure. *J. Biol. Chem.* **284,** 28624–28633
16. Heindl, C., Brune, K., and Renner, B. (2007) Kinetics and functional characterization of the glycine receptor α2 and α3 subunit. *Neurosci. Lett.* **429,** 59–63
17. Yévenes, G. E., and Zeilhofer, H. U. (2011) Molecular sites for the positive allosteric modulation of glycine receptors by endocannabinoids. *PLoS ONE* **6,** e23886
18. Gielen, M., Thomas, P., and Smart, T. G. (2015) The desensitization gate of inhibitory Cys-loop receptors. *Nat. Commun.* **6,** 6829
19. Jones, M. V., and Westbrook, G. L. (1996) The impact of receptor desensitization on fast synaptic transmission. *Trends Neurosci.* **19,** 96–101
20. Papke, D., and Grosman, C. (2014) The role of intracellular linkers in gating and desensitization of human pentameric ligand-gated ion channels. *J. Neurosci.* **34,** 7238–7252
21. Faber, D. S., and Korn, H. (1987) Voltage-dependence of glycine-activated Cl- channels: a potentiometer for inhibition? *J. Neurosci.* **7,** 807–811
22. Moroni, M., Biro, I., Giugliano, M., Vijayan, R., Biggin, P. C., Beato, M., and Sivilotti, L. G. (2011) Chloride ions in the pore of glycine and GABA channels shape the time course and voltage dependence of agonist currents. *J. Neurosci.* **31,** 14095–14106
23. Bormann, J., Hamill, O. P., and Sakmann, B. (1987) Mechanism of anion permeation through channels gated by glycine and gamma-aminobutyric acid in mouse cultured spinal neurones. *J. Physiol.* **385,** 243–286
24. Fatima-Shad, K., and Barry, P. H. (1993) Anion permeation in GABA- and glycine-gated channels of mammalian cultured hippocampal neurons. *Proc. Biol. Sci.* **253,** 69–75
25. Moorhouse, A. J., Keramidas, A., Zaykin, A., Schofield, P. R., and Barry, P. H. (2002) Single channel analysis of conductance and rectification in cation-selective, mutant glycine receptor channels. *J. Gen. Physiol.* **119,** 411–425
26. Keramidas, A., Moorhouse, A. J., Schofield, P. R., and Barry, P. H. (2004) Ligand-gated ion channels: mechanisms underlying ion selectivity. *Prog. Biophys. Mol. Biol.* **86,** 161–204
27. Keramidas, A., Moorhouse, A. J., Pierce, K. D., Schofield, P. R., and Barry, P. H. (2002) Cation-selective mutations in the M2 domain of the inhibitory glycine receptor channel reveal determinants of ion-charge selectivity. *J. Gen. Physiol.* **119,** 393–410
28. Sugiharto, S., Lewis, T. M., Moorhouse, A. J., Schofield, P. R., and Barry, P. H. (2008) Anion-cation permeability correlates with hydrated counterion size in glycine receptor channels. *Biophys. J.* **95,** 4698–4715
29. Du, J., Lü, W., Wu, S., Cheng, Y., and Gouaux, E. (2015) Glycine receptor mechanism elucidated by electron cryo-microscopy (2015) *Nature* **526,** 224–229
30. Strübing, C., Krapivinsky, G., Krapivinsky, L., and Clapham, D. E. (2001) TRPC1 and TRPC5 form a novel cation channel in mammalian brain. *Neuron* **29,** 645–655
31. Plant, T. D., and Schaefer, M. (2005) Receptor-operated cation channels formed by TRPC4 and TRPC5. *Naunyn Schmiedebergs Arch. Pharmacol.* **371,** 266–276
32. Lu, Z., and MacKinnon, R. (1994) Electrostatic tuning of Mg^{2+} affinity in an inward-rectifier K^+ channel. *Nature* **371,** 243–246
33. Fakler, B., Brändle, U., Glowatzki, E., Weidemann, S., Zenner, H. P., and Ruppersberg, J. P. (1995) Strong voltage-dependent inward rectification of inward rectifier K^+ channels is caused by intracellular spermine. *Cell* **80,** 149–154
34. Guo, D., Ramu, Y., Klem, A. M., and Lu, Z. (2003) Mechanism of rectification in inward-rectifier K^+ channels. *J. Gen. Physiol.* **121,** 261–275
35. Bordoli, L., Kiefer, F., Arnold, K., Benkert, P., Battey, J., and Schwede, T. (2009) Protein structure homology modeling using SWISS-MODEL workspace. *Nat. Protoc.* **4,** 1–13
36. Weltzien, F., Puller, C., O'Sullivan, G. A., Paarmann, I., and Betz, H. (2012) Distribution of the glycine receptor β-subunit in the mouse CNS as revealed by a novel monoclonal antibody. *J. Comp Neurol.* **520,** 3962–3981
37. Colquhoun, D. (1998) Binding, gating, affinity and efficacy: the interpretation of structure-activity relationships for agonists and of the effects of mutating receptors. *Br. J. Pharmacol.* **125,** 924–947
38. Lynch, J. W. (2004) Molecular structure and function of the glycine receptor chloride channel. *Physiol. Rev.* **84,** 1051–1095
39. Breitinger, H. G., Villmann, C., Rennert, J., Ballhausen, D., and Becker, C. M. (2002) Hydroxylated residues influence desensitization behaviour of recombinant α3 glycine receptor channels. *J. Neurochem.* **83,** 30–36
40. Meiselbach, H., Vogel, N., Langlhofer, G., Stangl, S., Schleyer, B., Bahnassawy, L., Sticht, H., Breitinger, H. G., Becker, C. M., and Villmann, C. (2014) Single expressed glycine receptor domains reconstitute functional ion channels without subunit-specific desensitization behavior. *J. Biol. Chem.* **289,** 29135–29147
41. Langlhofer, G., Janzen, D., Meiselbach, H., and Villmann, C. (2015) Length of the TM3-4 loop of the glycine receptor modulates receptor desensitization. *Neurosci. Lett.* **600,** 176–181
42. Legendre, P., Muller, E., Badiu, C. I., Meier, J., Vannier, C., and Triller, A. (2002) Desensitization of homomeric alpha1 glycine receptor increases with receptor density. *Mol. Pharmacol.* **62,** 817–827
43. Legendre, P. (1999) Voltage dependence of the glycine receptor-channel kinetics in the zebrafish hindbrain. *J. Neurophysiol.* **82,** 2120–2129
44. Chen, Z., and Huang, R. (2007) Identification of residues mediating inhibition of glycine receptors by protons. *Neuropharmacology* **52,** 1606–1615
45. Song, Y. P., Schlesinger, F., Ragancokova, D., Calixto, R., Dengler, R., and Krampfl, K. (2010) Changes in extracellular pH affect glycine receptor channels expressed in HEK 293 cells. *Eur. J. Pharmacol.* **636,** 59–64
46. Karlsson, U., Druzin, M., and Johansson, S. (2011) Cl(−) concentration changes and desensitization of GABA(A) and glycine receptors. *J. Gen. Physiol.* **138,** 609–626
47. Fucile, S., De Saint Jan, D., de Carvalho, L. P., and Bregestovski, P. (2000) Fast potentiation of glycine receptor channels by intracellular calcium in neurons and transfected cells. *Neuron* **28,** 571–583
48. Akaike, N., and Kaneda, M. (1989) Glycine-gated chloride current in acutely isolated rat hypothalamic neurons. *J. Neurophysiol.* **62,** 1400–1409
49. Miller, P. S., Harvey, R. J., and Smart, T. G. (2004) Differential agonist sensitivity of glycine receptor α2 subunit splice variants. *Br. J. Pharmacol.* **143,** 19–26
50. Yang, Z., Cromer, B. A., Harvey, R. J., Parker, M. W., and Lynch, J. W. (2007) A proposed structural basis for picrotoxinin and picrotin binding in the glycine receptor pore. *J. Neurochem.* **103,** 580–589
51. Chen, X., Cromer, B., Webb, T. I., Yang, Z., Hantke, J., Harvey, R. J., Parker, M. W., and Lynch, J. W. (2009) Dihydropyridine inhibition of the glycine receptor: subunit selectivity and a molecular determinant of inhibition. *Neuropharmacology* **56,** 318–327
52. Shan, Q., Han, L., and Lynch, J. W. (2012) Distinct properties of glycine receptor β+/α− interface: unambiguously characterizing heteromeric interface reconstituted in homomeric protein. *J. Biol. Chem.* **287,** 21244–21252
53. Saul, B., Kuner, T., Sobetzko, D., Brune, W., Hanefeld, F., Meinck, H. M., and Becker, C. M. (1999) Novel GLRA1 missense mutation (P250T) in dominant hyperekplexia defines an intracellular determinant of glycine receptor channel gating. *J. Neurosci.* **19,** 869–877
54. Bormann, J., Rundström, N., Betz, H., and Langosch, D. (1993) Residues within transmembrane segment M2 determine chloride conductance of glycine receptor homo- and hetero-oligomers *EMBO J.* **12,** 3729–3737; Correction (1994) *EMBO J.* **13,** 1493
55. Gundersen, C. B., Miledi, R., and Parker, I. (1984) Properties of human brain glycine receptors expressed in *Xenopus* oocytes. *Proc. R. Soc. Lond. B Biol. Sci.* **221,** 235–244

56. Zhang, Z. W., and Berg, D. K. (1995) Patch-clamp analysis of glycine-induced currents in chick ciliary ganglion neurons *J. Physiol.* **487,** 395–405
57. Keramidas, A., Moorhouse, A. J., French, C. R., Schofield, P. R., and Barry, P. H. (2000) M2 pore mutations convert the glycine receptor channel from being anion- to cation-selective. *Biophys. J.* **79,** 247–259
58. Zhorov, B. S., and Bregestovski, P. D. (2000) Chloride channels of glycine and GABA receptors with blockers: Monte Carlo minimization and structure-activity relationships. *Biophys. J.* **78,** 1786–1803
59. Eichler, S. A., Förstera, B., Smolinsky, B., Jüttner, R., Lehmann, T. N., Fähling, M., Schwarz, G., Legendre, P., and Meier, J. C. (2009) Splice-specific roles of glycine receptor α3 in the hippocampus. *Eur. J. Neurosci.* **30,** 1077–1091
60. Kubota, H., Alle, H., Betz, H., and Geiger, J. R. (2010) Presynaptic glycine receptors on hippocampal mossy fibers. *Biochem. Biophys. Res. Commun.* **393,** 587–591
61. Tabb, J. S., Kish, P. E., Van Dyke, R., and Ueda, T. (1992) Glutamate transport into synaptic vesicles. Roles of membrane potential, pH gradient, and intravesicular pH. *J. Biol. Chem.* **267,** 15412–15418
62. Cubelos, B., Giménez, C., and Zafra, F. (2005) Localization of the GLYT1 glycine transporter at glutamatergic synapses in the rat brain. *Cereb. Cortex* **15,** 448–459
63. Schenck, S., Wojcik, S. M., Brose, N., and Takamori, S. (2009) A chloride conductance in VGLUT1 underlies maximal glutamate loading into synaptic vesicles. *Nat. Neurosci.* **12,** 156–162
64. Förstera, B., a Dzaye, O. D., Winkelmann, A., Semtner, M., Benedetti, B., Markovic, D. S., Synowitz, M., Wend, P., Fähling, M., Junier, M. P., Glass, R., Kettenmann, H., and Meier, J. C. (2014) Intracellular glycine receptor function facilitates glioma formation *in vivo*. *J. Cell Sci.* **127,** 3687–3698
65. Förstera, B., Belaidi, A. A., Jüttner, R., Bernert, C., Tsokos, M., Lehmann, T. N., Horn, P., Dehnicke, C., Schwarz, G., and Meier, J. C. (2010) Irregular RNA splicing curtails postsynaptic gephyrin in the cornu ammonis of patients with epilepsy. *Brain* **133,** 3778–3794
66. Brewer, G. J., and Cotman, C. W. (1989) Survival and growth of hippocampal neurons in defined medium at low density: advantages of a sandwich culture technique or low oxygen. *Brain Res.* **494,** 65–74

Electrophysiological Signature of Homomeric and Heteromeric Glycine Receptor Channels

Constanze Raltschev, Florian Hetsch, Aline Winkelmann, Jochen C. Meier and Marcus Semtner

J. Biol. Chem. 2016, 291:18030-18040.
doi: 10.1074/jbc.M116.735084 originally published online July 5, 2016
